Paper No.
09446

NACE INTERNATIONAL | CORROSION 2009 CONFERENCE & EXPO

INTERNAL CURRENT EFFECTS ON LOCALIZED CORROSION RATE MEASUREMENTS USING COUPLED MULTIELECTRODE ARRAY SENSORS

Lietai Yang, Kuang-Tsan Kenneth Chiang, and Pavan K. Shukla
Southwest Research Institute®
6220 Culebra Rd
San Antonio, Texas 78238

Nobuo Shiratori
JGC Corporation
2205 Naritacho, Oaraimachi,
Higashi-Ibarakigun, Ibaraki Pref.
Japan

ABSTRACT

Coupled multielectrode arrays sensors (CMAS) have been used for real-time monitoring of corrosion, particularly localized corrosion. The internal anodic current on the most anodic electrode in a CMAS was evaluated for aluminum and carbon steel in simulated seawater and dilute HCl solutions. The Tafel extrapolation method was used to derive the internal currents on the most anodic electrode and the average corrosion current. In the simulated seawater, aluminum corroded dominantly in the form of localized corrosion and carbon steel corroded dominantly in the form of nonuniform general corrosion. In these cases, the externally measured nonuniform corrosion current on the most anodic electrode from the CMAS probe accounted for more than 90% of the total corrosion current. In the dilute HCl solution, both aluminum and carbon steel corroded dominantly in the form of uniform corrosion and the externally measured localized corrosion current on the most anodic electrode from the CMAS probe accounted for less than 56% of the total corrosion current.

It was concluded that if the externally measured nonuniform corrosion current from a CMAS probe is larger than the Tafel extrapolated currents, non-uniform corrosion is dominant and the effect of the internal current is not significant. In this case the CMAS probe reasonably measures the corrosion currents. However, if the externally measured nonuniform corrosion current from a CMAS probe is less than the Tafel extrapolated currents, uniform corrosion is dominant and the effect of the internal current may be significant. In this case, the CMAS probe only measures the nonuniform portion of the corrosion currents (which is not significant).

Therefore, CMAS probes are effective tools for corrosion monitoring in localized corrosion and nonuniform type of general corrosion. The unpolarized CMAS probes cannot be used to measure purely uniform type of general corrosion.

Keywords: Multielectrode sensor, corrosion monitoring, corrosion sensor, localized corrosion sensor, multielectrode array, nonuniform corrosion, coupled multielectrode.

INTRODUCTION

Coupled multielectrode systems have been used efficiently to provide high throughput test results in electrochemical studies and corrosion detection.[1] As early as 1977, Shibata and Takeyama used a coupled multielectrode system to evaluate the stochastic behavior of pitting corrosion.[2] Multiple specimens were connected to one potentiostat and polarized, and a large number of pitting potentials were obtained during one potentiodynamic scan. This approach greatly increased the efficiency for the pitting potential measurements and enabled the authors to study the stochastic behavior of the pitting corrosion of stainless steel. Later, Schiessl[3] coupled multielectrode systems for corrosion detection in concrete and Steinsmo and coworkers[4,5] used the systems for crevice corrosion measurements. Multiple electrodes of the same metal or different metals were placed in corrosive environments and connected to a common cathode. The anodic current from each electrode indicated the corrosion of the metals. If the electrodes were made of the same metal but placed in different locations, the coupled multielectrode system was used to detect the corrosion of the metal in the different locations. If the electrodes were made from different metals or the same metal with different heat treatment conditions but placed in the same electrolyte, the multielectrode system was used to produce a larger number of corrosion parameters in one experiment.

In 1996, Fei, et al.[6] used coupled multielectrodes in a novel way, arranging them in form of an array (or coupled multielectrode array) to study the spatial corrosion and electrochemical behavior of iron. In this approach, the coupled multielectrode array simulated a single piece of iron in a sulfuric acid solution. The authors determined the spatial pattern of the active-passive electrochemical oscillations and how the oscillation wave front travels on one large iron electrode. Later, other authors extensively used similar coupled multielectrode arrays to study the localized corrosion of different metals.[7-21] Some researchers call the coupled multielectrode arrays a "wire beam electrode" (or WBE).[7,8]

The coupled multielectrode arrays were recently used as sensors (called coupled multielectrode array sensors or CMAS) for real-time monitoring of the rate of corrosion, particularly localized corrosion.[1,22-26] Coupled multielectrode systems are powerful tools for corrosion studies, and they can provide both temporal and spatial information on corrosion, especially localized corrosion in two dimensions. However, the large amount of data from a multielectrode system is often incomprehensible to plant or facility operators. The data must be greatly reduced to one or to a few simple parameters so that the multielectrode systems can be used as a sensor to provide real-time data to help plant or filed facility operations.

Figure 1 shows the schematic diagram for a typical measuring circuit of the CMAS system.[27] Electrons from a corroding (or a relatively more corroding) electrode (or an anodic half-cell) flow to the common coupling joint and are individually measured by an instrument. The instrument imposes near zero voltage between each electrode and the coupling joint so

`

that all electrodes are at the same electrochemical potential and simulate the electrochemical behavior of a one-piece metal if the electrodes are close to each other. The corrosion current from the most anodic electrode (or the electrode that has the maximum anodic current) is often used to derive the localized corrosion rate (often called maximum localized corrosion rate). The maximum localized corrosion rate is one of the few simple parameters usually provided by a commercial CMAS instrument. Because the collection of the electrodes simulates a single piece of metal if the spacing between the electrodes is close enough, the most corroding electrode simulates the fast growing pit on this metal, if the localized corrosion is in the form of pitting corrosion and the size of the pit is close to the size of the electrode. The use of a few parameters, instead of the massive number of currents from a CMAS probe, as a localized corrosion parameter makes the CMAS easily usable for field applications. If the corrosion is wave-form general corrosion, rather than localized corrosion, the maximum localized corrosion rate represents the maximum nonuniform corrosion rate.

As mentioned above, the maximum localized corrosion rate is usually derived from the most anodic electrode by assuming the corrosion on this electrode is uniform (e.g., the pit reaches the dimension of the electrode). It is sufficient to examine the electrochemical behavior of the most anodic electrode and the cathodic electrodes that support the cathodic currents from the most anodic electrode during the measurement. Figure 2 shows the schematic diagram for the polarization curves of the most anodic electrode and several other cathodic electrodes, assuming that the anodic current from the single anodic electrode is supported by the cathodic currents from several cathodic electrodes during coupling.[1] Because localized corrosion often involves small areas of corroded anodic sites accompanied by large areas of cathodic sites, this assumption is reasonable in many environments. The thin solid curves in Figure 2 represent the dissolution and reduction polarization behaviors on the anodic electrode. The thick solid curves represent the combined dissolution and reduction polarization behaviors on the rest of the electrodes (the cathodic electrodes) if these cathodic electrodes are coupled as a single electrode.   For a passive metal, in the cathodic area (or the cathodic electrodes in a CMAS probe) where no localized corrosion has been initiated, the anodic current is usually extremely low due to the protective layer of oxide formed on the metal and the corrosion potential for the cathodic electrodes, E^c_{corr}, is high (or noble). For the anodic electrode where localized corrosion has been initiated and the protective layer has been compromised, the anodic current is usually high and the corrosion potential for the anodic electrode, E^a_{corr}, is low (or active). Note in Figure 2, the cathodic current on the combined cathodic electrodes is significantly higher than that on the anodic electrode. This is because we have assumed that the surface area on the anodic electrode is significantly smaller than that of the cathodic electrodes (one anodic electrode versus many cathodic electrodes). In addition, the cathodic reactions that would take place deep in a pit on the anodic electrode require more effort for the reactants (O_2 or H^+) to overcome the mass transfer barrier formed by the corrosion products that covers the pit.

When the most anodic electrode and the combined cathodic electrodes are coupled, the corrosion potential changes to a new value, E_{coup} (or E_{corr} for all coupled electrodes), and the total anodic dissolution currents equal the total cathodic reduction currents[28]:

$$\sum I_{Dissolution} = \sum I_{Reduction} \tag{1a}$$

or

$$|I_{corr}| + |I^c_{in}| = |I^a_{in}| + |I^c| \tag{1b}$$

`

3

where I_{corr} is the corrosion current (dissolution current) on the anodic electrode; I^c_{in} is the dissolution (anodic) current on the combined cathodic electrodes (anodic current that flows within all the cathodes); I^a_{in} is the internal anodic current, which equals the internal cathodic current on the anodic electrode (the currents that flow within the anode); and I^c is the cathodic current on the combined cathodic electrodes.

On the anodic electrode, the corrosion current (total dissolution current), I_{corr}, is equal to the sum of the externally flowing anodic current, I_{ex}, and the internally flowing anodic current, I^a_{in}. Therefore,

$$I_{corr} = I_{ex} + |I^a_{in}| \qquad (2)$$

Because the I^a_{in} for the anodic electrode, especially when the anodic electrode is the most anodic electrode of the CMAS probe,[1] is often much less than its I_{ex} at the coupling potential in a localized corrosion environment, the externally flowing current from such an anodic electrode of the probe can often be directly used to estimate the localized corrosion current:

$$I_{corr} \approx I_{ex} \qquad (3)$$

In cases where the environment is not corrosive or localized corrosion is not dominant, when compared with the uniform corrosion, there would be less separation between the anodic electrodes and the cathodic electrodes. The behavior of even the most anodic electrode may be similar to the other electrodes in the CMAS probe. In this case, the I^a_{in} for the anodic electrode would be close to I_{ex} and I^c_{in} would be close to I^c.

In assessing the effect of internal currents on localized corrosion measurement using a CMAS probe, the authors proposed using the Tafel extrapolation method to estimate the I^a_{in} for the most anodic electrode.[29, 30] This paper provides additional data to evaluate the internal current effect on the measurement of nonuniform corrosion (especially localized corrosion) with CMAS probes.

EXPERIMENTS

A 16-electrode aluminum CMAS probe and a 16-electrode carbon steel CMAS probe were used in the test. The sensing electrodes were Type 1100 aluminum (UNS A91100) and Type 1018 carbon steel (UNS G10180) wires for the aluminum and carbon steel probes, respectively. Both wires were 1 mm in diameter. The spacing between the electrodes was approximately 2 mm. According to the Ohmic potential field distribution calculated for a flush mounted electrode of 0.15 mm diameter in a 1 mS/cm solution,[17,28] the potential drop from the electrode to the solution at a distance of 2 mm is less than 500 mV if the current density is 0.1 A/cm^2. The conductivity of the solution in the monitoring system is usually higher than 1 mS/cm (approximately 100 mS/cm for seawater and 1 to 20 mS/cm for cooling water).[31] The maximum current density form a CMAS probe is usually less than 0.3 mA/cm^2 in sweater and 0.03 mA/cm^2 in cooling water, the potential drop caused by solution resistance is expected to be less than 0.1 mV, which is not significant.

---

[1]Note: The most anodic electrode is the electrode that has the highest anodic current; it is also called the most corroding electrode.[1]

`

Prior to each test, the sensing surface of the CMAS probe (the tip of the probe) was polished with 400-grit sand paper and cleaned with acetone. The experimental setup up is shown in Figure 3. The experimental procedure has been described in a recent conference proceeding[30] and is also given as follows.

The potentiostat was a model SI1287A[TM].[(2)] The CMAS analyzer was an 18-channel (A-18) nanoCorr[TM(3)] that was interfaced with a computer with CorrVisual[TM] software for automated data acquisition. The working electrode post of the potentiostat was connected to the coupling joint of the CMAS analyzer. Because the coupling joint is connected to all the electrodes of the CMAS probe, these electrodes can be polarized by the potentiostat during the polarization test. The CMAS analyzer acted essentially as a multichannel zero-voltage ammeter (an ammeter that produces a negligible effect on the potential of the electrode when it is inserted into the circuit to measure the current from the electrode). The reference electrode was a saturated calomel electrode (SCE), and the counter electrode was a stainless steel rod. In addition to being connected to the potentiostat, the reference electrode was also connected to the reference electrode post of the CMAS analyzer. The potentiostat provided the required potentiodynamic polarization to the probe electrodes. The CMAS analyzer gathered all the data, including probe potential and currents for all electrodes during the experiment.

The experiments were conducted in a beaker filled with either simulated seawater (3 wt% NaCl solution), a 0.2 wt% HCl solution or a 2 wt% HCl solution at room temperature (23 ^{o}C) without agitation. The solutions were prepared with reagent-grade chemicals and 18.2 Mohm-cm deionized water. The solutions were not purged and were expected to contain oxygen near saturation level. During the test, the electrodes of the CMAS probe under testing were first held at open-circuit potential (coupling potential of the probe) for about 2 hours prior to the polarization test. Then the electrodes were potentiodynamically polarized, starting from the open-circuit potential toward the cathodic direction at a scan rate of 0.167 mV/sec. The end potential was 500 mV below the open-circuit potential of the probe. Figure 4 shows typical potential and individual currents from one of the CMAS probes prior to, during, and after the cathodic polarization test. When the electrodes of the probe were at the natural coupling potential (with no polarization by the potentiostat), the collection of the electrodes simulated the behavior of a single piece of metal. Some electrodes were anodic and some were cathodic; the average current was zero. The highest anodic current is the maximum corrosion current measured with the CMAS probe, and its value is often used to calculate the maximum corrosion rate for localized corrosion or nonuniform general corrosion.

RESULTS

Figure 5 shows the individual currents as a function of the probe potential during the cathodic scan for the aluminum probe in the 3 wt% NaCl solution. The anodic currents started to decrease upon the start of the cathodic scan and became negative after the potential was below the corrosion potentials of the individual electrodes (E^{i}_{corr}, where i is the ith electrode). The average current changed from zero to a negative value during the cathodic scan.

[(2)]SI 1287A is a trademark of Solartron Analytical.
[(3)]nanoCorr and CorrVisual are trademarks of Corr Instruments.

`

Figure 6 shows the logarithm of the absolute currents from the individual electrodes of the aluminum CMAS probe as a function of the potential in the simulated seawater.

For corrosion processes that are activation controlled, and if the cathodic reactions taking place during the cathodic polarization are the same as the reactions taking place at the corrosion potentials, Tafel equation (Tafel extrapolation) may be used to derive the corrosion current:[31]

$$E - E_{corr} = b_c \log(I/I_{corr}) \qquad (4)$$

where E is the electrode potential, E_{corr} is the corrosion potential ($E-E_{corr}$ is the overpotential), b_c is the Tafel slope for cathodic polarization, I is the measured polarization current, and I_{corr} is the corrosion current. When $\log(I)$ is plotted against E, $\log(I_{corr})$ can be obtained by extrapolating the linear relationship at the large overpotential section (100 to 500 mV lower than the corrosion potential) to the corrosion potential. The extrapolation method is also applicable to the corrosion process that is totally controlled by diffusion because the current is a constant and the $\log(I)$ versus E relationship is a vertical line. For corrosion that is controlled by both diffusion and activation processes, the Tafel extrapolation method may be used to approximate the corrosion current.

Therefore, when applied to the average corrosion current, the Tafel extrapolation method may be used to derive the general corrosion rate of the metal at the corrosion potential (which equals the coupling potential for an unpolarized CMAS probe). Because the internal anodic current equals the internal cathodic current on the most anodic electrode at the coupling potential, Tafel extrapolation based on the cathodic curve from the most anodic electrode may be used to estimate the internal anodic current on the most anodic electrode (I^a_{in}). [29,30] Figure 7 shows the Tafel extrapolations for the cathodic polarization current from the most anodic electrode and for the average cathodic current for all the electrodes on the CMAS probe to the coupling potential. The data used for the linear extrapolation were between 100 and 500 mV below the coupling potential of the probe. According to Figure 7, the externally measured anodic current from the most anodic electrode, which has been called the maximum localized corrosion current from the CMAS probe[1] ($I_{ex,MAE}$), is 4.27E-7 A (see also Figures 5 and 6), the internal anodic current on the most anodic electrode ($I^a_{in,MAE}$) is 2.5E-8 A, and the average corrosion current ($I_{corr,AVG}$) is 4.1E-8 A.

Figure 8 shows the typical polarization curves for the electrodes on the aluminum CMAS probe in an air-saturated 0.2 wt% HCl solution and the Tafel extrapolation parameters for the current from the most anodic electrode and for the average current. The values of $I_{ex,MAE}$, $I^a_{in,MAE}$, and $I_{corr,AVG}$ are also shown in Figure 8. Noted that the value of $I^a_{in,MAE}$ is higher than $I_{corr,AVG}$, which is uncommon (see Figure 7, Figure 9 described in the next paragraph, and the previously published data[30]) because the most anodic electrode is often covered by a layer of corrosion products, giving the most anodic electrode a higher mass-transfer resistance than the average electrodes.

Figure 9 shows the typical polarization curves for the electrodes on the carbon steel CMAS probe in an air-saturated 2 wt% HCl solution and the Tafel extrapolation parameters for the current from the most anodic electrode and for the average current. The corresponding values of $I_{ex,MAE}$, $I^a_{in,MAE}$, and $I_{corr,AVG}$ are also shown in Figure 9.

`

DISCUSSION

Estimation of the Internal Anodic Current

If the coupling potential is close to the corrosion potential of the most anodic electrode, the internal current on the most corroding electrode at the coupling potential may also be estimated by the corrosion current on the most anodic electrode at its corrosion potential. If the corrosion process is activation controlled, the corrosion current on the most anodic electrode may be obtained with the widely used Stern-Gary equation [the linear polarization resistance (LPR) method]:[31]

$$I_{corr} = B/R_p \tag{5}$$

where B is a constant determined by the anodic and cathodic Tafel slopes and R_p is the slope of the E versus I plot near the corrosion potential.

Table 1 shows the corrosion rate measured with the LPR method and comparisons with the values obtained with the Tafel extrapolation method. The LPR data in 3 wt% NaCl and 0.2 wt% solution was obtained previously,[30] and the LPR data in the 2 wt% HCl solution was obtained from Figure 9 for Electrode No.13 near its corrosion potential. The B value was the same as the one used for carbon steel in 0.2 wt% HCl solution as described previously (20 mV).[30] There are excellent agreements between the LPR data and the Tafel extrapolated data for the 3 wt% NaCl and 0.2 wt% HCl solutions. However, in the 2 wt% HCl solution, the Tafel extrapolation value is 4.5 times higher than the LPR data. The large discrepancy may be due to the large variations in corrosion rates from specimens to specimens or due to the variations in the two methods. Even for the same method, data may vary significantly from one experiment to another. An example is the corrosion rates measured with the LPR method for Alloy 22 in a brine solution at ambient temperature.[32] These measurements (approximately 50 data points) were conducted with the same type of Alloy 22 electrode over a period of 125 days. These data varied from 8 to 35 nm/yr. Therefore, corrosion rate measurements may vary significantly even with the same method for the same type of specimens in the same solution. A large number of measurements are required to obtain meaningful representative results. Compared with this example, a difference of 4.5 times for the corrosion rate data that are obtained with different methods is not surprising. As a mater of fact, both the LPR and the Tafel extrapolation methods were developed based on the assumption that the activation process is the controlling step. The data for the HCl solution should have been more reliable than the data for the NaCl solution because oxygen mass-transfer plays a more important role for carbon steel corrosion in air-saturated NaCl solution than in diluted HCl solution in which the carbon steel corrosion is dominated by activation-controlled uniform corrosion.[33]

Effect of Internal Anodic Current

The total corrosion current on the most anodic electrode at the coupling potential can be calculated according to Eq. 6:

$$I_{corr,MAE} = I_{ex,MAE} + |I^a_{in,MAE}| \tag{6}$$

`

where MAE means that the parameters are for the most anodic electrode (MAE) in a CMAS probe. Because $I_{corr,MAE}$ is the total corrosion current on the most corroding electrode (the electrode that has the highest corrosion rate on a CMAS probe), this current may be used to represent the localized corrosion current for the metal if the corrosion mode is localized corrosion or the maximum corrosion current if the corrosion is wavelike (nonuniform) general corrosion assuming that the corrosion on the most anodic electrode is uniform. It should be mentioned that the uniform assumption may cause errors if the electrode is large and the corroded section is small, especially for cases where only small number of small pits initiate and grow preferentially in the depth direction.[22] It has been demonstrated that the surface of the most corroded electrode of 1 mm in diameter was completely corroded in the cases for carbon steel in sea water[34] and cooling water[35] and stainless steel in $FeCl_3$-contianing solutions.

Table 2 shows the total corrosion currents ($I_{corr,MAE}$); externally measured anodic currents from the most anodic electrode ($I_{ex,MAE}$); the estimated internal anodic currents for the most anodic electrodes ($I^a_{in,MAE}$); and the average corrosion current ($I_{corr, AVG}$) obtained from Figures 7 and 8 for aluminum, Figure 9, and previously published figures[30] for carbon steel in several environments.

Table 2 also presents the ratio of $I_{ex,MAE}/I_{corr,MAE}$, $I^a_{in, MAE}/I_{corr,MAE}$, and $I_{corr,MAE}/I_{corr,AVG}$. The ratio of $I^a_{in, MAE}/I_{corr,MAE}$ indicates the percentage effect of the internal anodic current, which is not directly measurable, on the measurement of the nonuniform corrosion rate on the most anodic electrode. The ratio of $I_{ex,MAE}/I_{corr,MAE}$ indicates how close the externally measured anodic current from the CMAS probe is to the corrosion current on the most anodic electrode. The two ratios are related to each other because the sum of the two ratios is one. In simulated seawater, the values of $I^a_{in, MAE}/I_{corr,MAE}$ are low (<10%) for both aluminum and carbon steel, indicating that the internal anodic current effect is insignificant and the externally measured anodic current from the CMAS probe can adequately approximate the corrosion current on the most anodic electrode. For carbon steel in 2 wt% HCl solution and for aluminum in 0.2 wt% HCl solution, the values of $I^a_{in, MAE}/I_{corr,MAE}$ are high (>75%), indicating that the internal anodic current effect is severe and the externally measured anodic current from the CMAS probe cannot be used to approximate the corrosion current on the most anodic electrode. For carbon steel in the 0.2 wt% HCl solution, the $I^a_{in, MAE}/I_{corr,MAE}$ value is 44%, indicating that the internal anodic current effect is significant and the externally measured anodic current from the CMAS probe may be used to approximate the corrosion current on the most anodic electrode, but the error may be significant (44%). Noted that the error of 44% is exceptionally large for the measurement of most types of industrial process parameters such as temperature and pressure, but it is not a large number when corrosion rate is concerned (see the aforementioned example where 300% to 400% of variation was observed for the 50 data points obtained with the same metal, same solution, and same LPR method). The large variation is true especially when localized corrosion is concerned. In addition, evaluation of pitted metal specimens after exposures in a corrosive industrial environment revealed that the maximum pit depth often varies from one coupon to another by multiple factors.[35]

Severity of Nonuniform Corrosion

In addition, Table 2 also presents the ratio of $I_{corr,MAE}/I_{corr,Avg}$, which indicates the degree of localized or nonuniform corrosion or how much faster the most anodic electrode corrodes than an average electrode corrodes. A similar ratio has been used in other publications.[36] This

`

term was borrowed originally from a term used in the American Society of Testing and Materials Standard (ASTM G46)[37]— pitting factor—which is defined as the ratio of deepest metal penetration to average metal penetration in a exposed coupon. Currently, there is no standard criterion for the characterization of localized corrosion severity based on the pitting factor. The following arbitrary criterion is proposed to analyze the data presented in this paper:

Benign nonuniform (or localized) corrosion: $I_{corr,MAE}/I_{corr,Avg} < 3$

Moderate nonuniform (or localized) corrosion: $3 < I_{corr,MAE}/I_{corr,Avg} < 5$

Severe nonuniform (or localized) corrosion: $I_{corr,MAE}/I_{corr,Avg} > 5$

If $I_{corr,MAE}/I_{corr,Avg} < 3$, the nonuniform corrosion is considered to be benign because the ultimate long-term outcome is uniform or slightly wave-form general corrosion[38] even if the corrosion started as localized corrosion.

The $I_{corr, MAE}/I_{corr, Avg}$ value for carbon steel in the 2 wt% HCl solution in Table 2 should be greater than 1. The low value (0.89) reflects the large errors in obtaining the $I^a_{in, MAE}$ and $I_{corr, Avg}$ values using the Tafel extrapolation method. Slight changes in the extrapolation slope would make this ratio significantly different and cause large errors for the ratio in cases where $I_{ex, MAE}$ is substantially less than $I^a_{in, MAE}$ or $I_{corr,AVG.}$

Summary for Effect of Internal Anodic Current

Figure 10 compares all previously mentioned case behaviors. In a highly localized corrosion environment (Figure 10a for aluminum in 3 wt% NaCl), the internal current on the most anodic electrode is lower than the average corrosion current derived from all electrodes ($I^a_{in, MAE} < I_{corr,Avg}$) and the externally measured anodic current from the most anodic electrode of the CMAS probe is clearly larger than the average corrosion current ($I_{ex,MAE} >> I_{corr,MAE}$). The internal current is negligibly small (<10%) compared with the total corrosion current or externally measured anodic current from the most anodic electrode. Therefore, a CMAS probe is an effective tool in monitoring localized corrosion.

In an environment that causes general corrosion with significant nonuniform corrosion (Figure 10b for carbon steel in 3% NaCl), the internal current on the most anodic electrode is also lower than the average corrosion current derived from all electrodes ($I^a_{in, MAE} < I_{corr,Avg}$) and the externally measured anodic current from most anodic electrode of the CMAS probe is also clearly larger than the average corrosion current ($I_{ex,MAE} >> I_{corr,MAE}$). The internal current is also negligibly small (<10%) compared with the total corrosion current or externally measured anodic current from the most anodic electrode. Therefore, a CMAS probe is also an effective tool in monitoring general corrosion in an environment where nonuniform corrosion is significant.

In environments that cause general corrosion dominated by uniform corrosion (Figures 10c for aluminum in 0.2% HCl solution, Figure 10d for carbon steel in 2% HCl solution, and Figure 10e for carbon steel in 0.2% HCl solution), the CMAS probe only measures the nonuniform portion of the corrosion.

As an overall criterion, if the externally measured nonuniform corrosion current is larger than the Tafel extrapolated currents as shown in Figures 10a and 10b ($I_{ex,MAE} > I^a_{in,MAE}$ or $I_{ex,MAE} > I_{corr,AVG}$), the effect of internal current is not significant and the CMAS probe effectively

`

measures the corrosion currents. If the externally measured nonuniform corrosion current is less than the Tafel extrapolated currents as shown in Figures 10c and 10d ($I_{ex,MAE} < I^a_{in,MAE}$ or $I_{ex,MAE} < I_{corr,AVG}$), the effect of internal current is significant and the CMAS probe only measures the nonuniform portion of the corrosion currents.

CONCLUSIONS

The internal anodic current on the most anodic electrode in a coupled multielectrode array sensor was evaluated for aluminum and carbon steel in simulated seawater and dilute HCl solutions. The Tafel extrapolation method was used to derive the internal currents on the most anodic electrode and the average corrosion current. In the simulated seawater, aluminum corroded dominantly in the form of localized corrosion, and carbon steel corroded dominantly in the form of nonuniform general corrosion. In these cases, the externally measured nonuniform corrosion current accounted for more than 90% of the total corrosion current on the most anodic electrode. However, in the dilute HCl solutions, both aluminum and carbon steel corroded dominantly in the form of uniform corrosion and the externally measured localized corrosion current accounted for less than 56% of the total corrosion current on the most anodic electrode.

As an overall criterion, if the externally measured nonuniform corrosion current from a CMAS probe is larger than the Tafel extrapolated currents, the effect of internal current is not significant and the CMAS probe effectively measures the corrosion currents. If the externally measured nonuniform corrosion current from a CMAS probe is less than the Tafel extrapolated currents, the effect of internal current may be significant and the CMAS probe only measures the nonuniform portion of the corrosion currents.

ACKNOWLEDGMENTS

REFERENCES

1.   L. Yang, "Multielectrode Systems," in "Corrosion Monitoring Techniques," L. Yang, ed., Woodhead Publishing, Success, UK, (2008), Chapter 8.

2.   T. Shibata and T. Takeyama, "Stochastic Theory of Pitting Corrosion," Corrosion, 33, (1977), p. 243-251.

3.   P. Schiessl, United States Patent 5,015,355, "Corrosion Measuring Cell," May 14, 1991.

4.   U. Steinsmo, "The Effect of Temperature on Propagation of Crevice Corrosion of High Alloyed Stainless Steel in Natural Seawater," Progress in the Understanding and Prevention of Corrosion, 10th Eur. Corros. Congr. Paper, Volume 2, J.M. Costa and A.D. Mercer, eds., Institute of Materials, London, UK, 1993, p. 974-982.

`

5.   U. Steinsmo, T. Rone, and J.M. Drugli, "Aspects of Testing and Selecting Stainless Steels for Sea Water Applications," CORROSION/94, paper no. 492, (Houston, TX: NACE International, 1994).

6   Z. Fei, R.G. Kelly, and J.L. Hudson, "Spatiotemporal Patterns on Electrode Arrays," J. Phys. Chem., 100, (1996), p. 18986-18991.

7.   Y.J. Tan, "Monitoring Localized Corrosion Processes and Estimating Localized Corrosion Rates Using a Wire-beam Electrode," Corrosion, 54 (5) (1998), p. 403-413.

8.   Y.J. Tan, "Wire Beam Electrode: A New Tool for Studying Localized Corrosion and Other Inheterogeneity Electrochemical Processes," Corrosion Science, 41 (2) (1999), p. 229-247.

9.   Y.J. Tan, S. Bailey, B. Kinsella, and A. Lowe, "Mapping Corrosion Kinetics Using the Wire Beam Electrode in Conjunction with Electrochemical Noise Resistance Measurements," Journal of the Electrochemical Society, 147 (2) (2000), p. 530-540.

10.   Y.J. Tan, S. Bailey, and B. Kinsella, "Mapping Nonuniform Corrosion in Practical Corrosive Environments Using the Wire Beam Electrode Method (I) - Multi-phase Corrosion," Corrosion Science, 43 (2001), p. 1905-1918.

11.   Y.J. Tan, S. Bailey, and B. Kinsella, "Mapping Nonuniform Corrosion in Practical Corrosive Environments Using the Wire Beam Electrode Method (II) - Crevice Corrosion," Corrosion Science, 43 (2001), p. 1919-1929.

12.   Y.J. Tan, S. Bailey, and B. Kinsella, "Mapping Nonuniform Corrosion in Practical Corrosive Environments Using the Wire Beam Electrode Method (III) — Water-line Corrosion," Corrosion Science, 43 (2001), p. 1930-1937.

13.   Y.J. Tan, "Measuring Localized Corrosion Using the Wire Beam Electrode Method," in special Electrochemical Society publication: "Corrosion Science: A Retrospective and Current Status," the Electrochemical Society 201st Meeting, Philadelphia, USA, (2002) p. 377-384.

14.   N.N. Aung and Y.J. Tan, "A New Method of Studying Buried Steel Corrosion and Its Inhibition Using the Wire Beam Electrode," Corrosion Science, 46 (2004), p. 3057-3067.

15.   T.T. Lunt, J.R. Scully, V. Brusamarello, A.S. Mikhailov, and J.L. Hudson, "Spatial Interactions Among Localized Corrosion Sites: Experiments and Modeling," J. Electrochemical Soc. 149 (5) (2002), p. B163-B173.

16.   N.D. Budiansky, J.L. Hudson, and J.R. Scully, "Origins of Persistent Interaction Among Localized Corrosion Sites on Stainless Steel," Journal of the Electrochemical Society, 151 (4) (2004), p. B233-B243.

17.   N.D. Budiansky, F. Bocher, H. Cong, M.F. Hurley, and J.R. Scully, "Use of Coupled Multi-Electrode Arrays to Advance the Understanding of Selected Corrosion Phenomena," CORROSION/2006, paper no. 06677 (Houston, TX: NACE, 2006).

`

18.   H. Cong, N.D. Budiansky, J.R. Scully, and H.T. Michels, "Use of Coupled Electrode Arrays to Elucidate Copper Pitting as a Function of Potable Water Chemistry," CORROSION/07, paper no. 07392 (Houston, TX: NACE, 2007).

19.   F.D. Wall and M.A. Martinez, "A Statistics-Based Approach to Studying Aluminum Pit Initiation–Intrinsic and Defect-Driven Pit Initiation Phenomena," Journal of the Electrochemical Society, 150 (4) (2003), p. B146-B157.

20.   F.D. Wall, C.M. Johnson, J.C. Barbour, and M.A. Martinez, "The Effects of Chloride Implantation on Pit Initiation in Aluminum," Journal of The Electrochemical Society, 151 (2) (2004), p. B77-B81.

21.   F.D. Wall, M.A. Martinez, and J.J. Van den Avyle, "Relationship Between Induction Time for Pitting and Pitting Potential for High-Purity Aluminum," Journal of the Electrochemical Society, 151 (6) (2004), p. B354-B358.

22.   L. Yang, N. Sridhar, O. Pensado, and D. Dunn, "An In-Situ Galvanically Coupled Multi-Electrode Array Sensor for Localized Corrosion," Corrosion, 58 (2002), p. 1004.

23.   L. Yang and N. Sridhar, "Monitoring of Localized Corrosion," in ASM Handbook, Volume 13A-Corrosion: Fundamentals, Testing, and Protection, S.D. Crammer and B.S. Covino, Jr., eds., ASM International, Materials Park, Ohio, (2003), p. 519-524.

24.   L. Yang, N. Sridhar, C.S. Brossia, and D.S. Dunn, "Evaluation of the Coupled Multielectrode Array Sensor as a Real Time Corrosion Monitor," Corrosion Science, 47 (2005), p. 1794-1809.

25.   A. Anderko, N. Sridhar, L. Yang, S.L. Grise, B.J. Saldanha, and M.H. Dorsey, "Validation of a Localized Corrosion Model Using Real-Time Corrosion Monitoring in a Chemical Plant," Corrosion Engineering, Science and Technology (formerly British Corrosion J.), 40 (1) (2005) p. 33-42.

26.   B. Yang, F.J., Marinho, A.V. Gershun, "New Electrochemical Methods for the Evaluation of Localized Corrosion in Engine Coolants," Journal of ASTM International, 4(1) (2007), paper ID JAI100502 (Available online at www.astm.org).

27.   X. Sun and L. Yang, "Real-Time Monitoring of Localized and General Corrosion Rates in Drinking Water Utilizing Coupled Multielectrode Array Sensors," CORROSION/2006, paper no. 06094 (Houston, TX: NACE International, 2006).

28.   H. Cong, F. Bocher, N. D. Budiansky, M. F. Hurley, and J. R. Scully, "Use of Coupled Multi-Electrode Arrays to Advance the Understanding of Selected Corrosion Phenomena", Journal of ASTM International, Vol. 4, No. 10 Paper ID JAI101248, Available online at www.astm.org.

29.   L. Yang and K.T. Chiang, "A Review of Coupled Multielectrode Array Sensors for Corrosion Monitoring and a Study on the Behaviors of the Anodic and Cathodic Electrodes," submitted to Journal of ASTM, 2008.

`

30.　L. Yang and K.T. Chiang, "Electrochemical Behavior and Internal Current of the Most Anodic Electrode in a Coupled Multielectrode Array Sensor," Proceedings of the 17th International Corrosion Congress, 2008.

31　S. Papavinasam, "Electrochemical Techniques for Corrosion Monitoring," in "Corrosion Monitoring Techniques," L. Yang, ed., Woodhead Publishing, Success, UK (2008), Chapter 3.

32.　Sandia National Laboratories, "General Corrosion and Localized Corrosion of Waste Package Outer Barrier," ANL–EBS–MD–000008. Rev. 03. p. 6-112, Las Vegas, Nevada: Sandia National Laboratories. 2007.

33.　G.P. Marsh, K.J. Taylor, I.D. Bland, C. Westcott, P.W. Tasker, and S.M. Sharland, "Evaluation of the Localized Corrosion of Carbon Steel Overpacks for Nuclear Waste Disposal in Granite Environments," in Proceedings, Vol. 59, The Materials Research Society, Pittsburgh, Pennsylvania (1958), p. 421-428.

34.　N. Shiratori, N. Sridhar, L. Yang and D. S. Dunn, "Effect of Electrode Number and Size on Corrosion Rate Obtained from Coupled Multielectrode Array Sensor System", Proceedings of the 17th International Corrosion Congress, 2008.

35.　H. Dorsey, L. Yang, and N. Sridhar, "Cooling Water Monitoring Using Coupled Multielectrode Array Sensors and Other On-line Tools," CORROSION/2004, paper no. 04077 (Houston, TX: NACE International, 2004).

36.　X. Sun and L. Yang, "Real-Time Monitoring of Localized and General Corrosion Rates in Simulated Marine Environments Using Coupled Multielectrode Array Sensors," CORROSION/2006, paper no. 06284 (Houston, TX: NACE International, 2006).

37.　ASTM G46, "Standard Guide for Examination and Evaluation of Pitting Corrosion," Annual Book of ASTM Standards, Vol.03.02, ASTM 100 Barr Harbor Drive, West Conshohocken, PA 19428 (2008).

38.　G. Cragnolino, "Corrosion Fundamentals and Characterization Techniques," in "Corrosion Monitoring Techniques," L. Yang, ed., Woodhead Publishing, Success, UK (2008), Chapter 2.

`

Table 1. Comparison of the Internal Anodic Currents for the Most Anodic Electrode of a Carbon Steel CMAS Probe at Coupling Potentials Estimated by LPR and Tafel Extrapolation Methods

	3 wt% NaCl*	0.2 wt% HCl*	2 wt% HCl**
Tafel Extrapolation Method (A)	2.10E-07	6.30E-07	4.57E-06
LPR Method (A)	2.00E-07	7.02E-07	1.03E-06
* Data published previously[30] **Data from Figure 9 (7 data points from Electrode 9 near its corrosion potential gave a slope of 19492 V/A)			

Table 2. Corrosion Currents, Externally Measured Anodic Currents, and the Internal Anodic Currents for Most Anodic Electrodes and Average Corrosion Current for Aluminum and Carbon Steel CMAS Probes

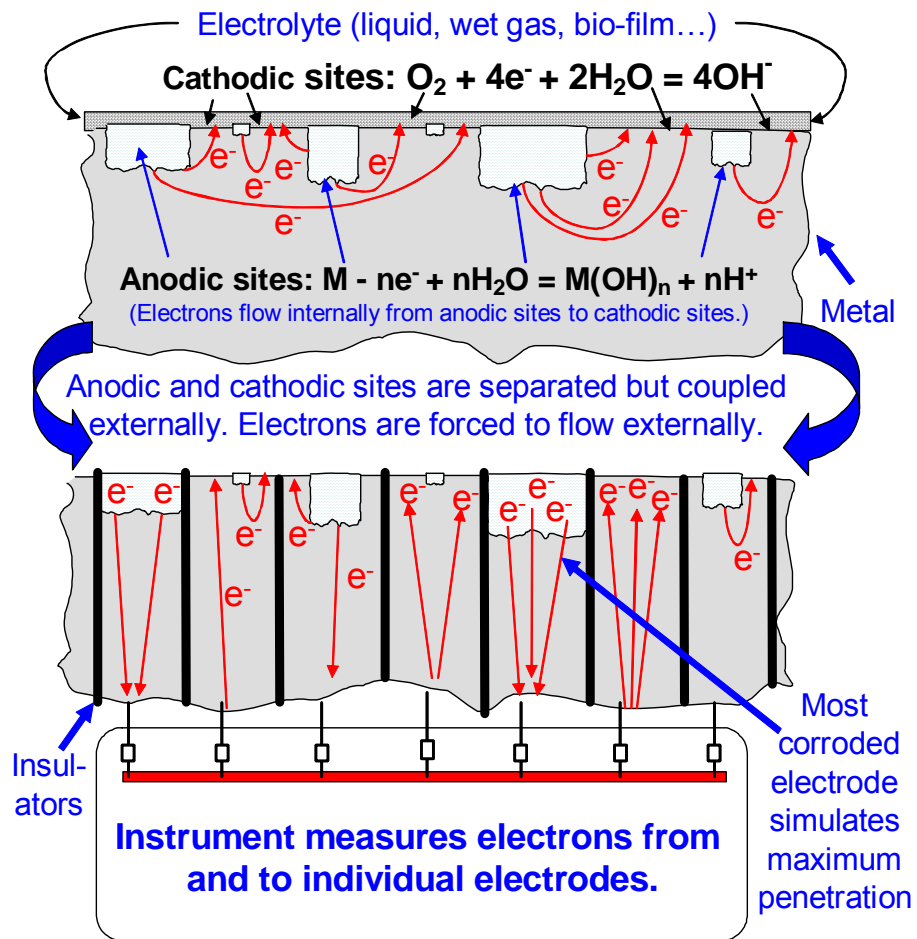|	Al in 3% NaCl	CS in 3% NaCl[#]	Al in 0.2% HCl	CS in 2% HCl	CS in 0.2 wt% HCl[#]
$I_{ex,MAE}$* (A)	4.27E-07	2.60E-06	4.36E-07	1.10E-06	7.94E-07
$I^a_{in,MAE}$	2.50E-08	2.10E-07	1.90E-06	3.90E-06	6.30E-07
$I_{corr,MAE}$** (A)	4.52E-07	2.81E-06	2.34E-06	5.00E-06	1.42E-06
$I_{corr,AVG}$$ (A)	4.10E-08	6.30E-07	8.70E-07	5.60E-06	1.00E-06
$I_{ex,MAE}/I_{corr,MAE}$	0.94	0.93	0.19	0.22	0.56
Effect of Internal Current ($I^a_{in,MAE}/I_{corr,MAE}$)	6%, Insignificant	7%, Insignificant	81%, Severe	78%, Severe	44%, Significant
$I_{corr,MAE}/I_{corr,AVG}$	11.02	4.46	2.69	0.89	1.42
Corrosion Mode	Localized	Nonuniform	Uniform	Uniform	Uniform
* $I_{ex,MAE}$—externally measured anodic current from most anodic electrode ** $I_{corr,MAE}$—Corrosion current on most anodic electrode ($I_{corr,MAE} = I_{ex,MAE} + I^a_{in,MAE}$) $ $I_{corr, AVG}$—average corrosion current on all electrodes $$ Value reflects errors in $I_{corr,MAE}$ and $I_{corr, AVG}$ (It should be greater than 1) # Data from previously published data[30]					

`

Electrolyte (liquid, wet gas, bio-film…)

Cathodic sites: $O_2 + 4e^- + 2H_2O = 4OH^-$

e^- e^- e^- e^- e^-
e^- e^- e^-
e^- e^- e^- e^-

Anodic sites: $M - ne^- + nH_2O = M(OH)_n + nH^+$
(Electrons flow internally from anodic sites to cathodic sites.)

Metal

Anodic and cathodic sites are separated but coupled externally. Electrons are forced to flow externally.

e^- e^- e^- e^- e^- e^- e^- e^- e^-
e^- e^- e^- e^-
e^- e^- e^-
e^-

Insul-
ators

Most
corroded
electrode
simulates
maximum
penetration

**Instrument measures electrons from
and to individual electrodes.**

Figure 1. Schematic diagram of the coupled multielectrode array system.[27]
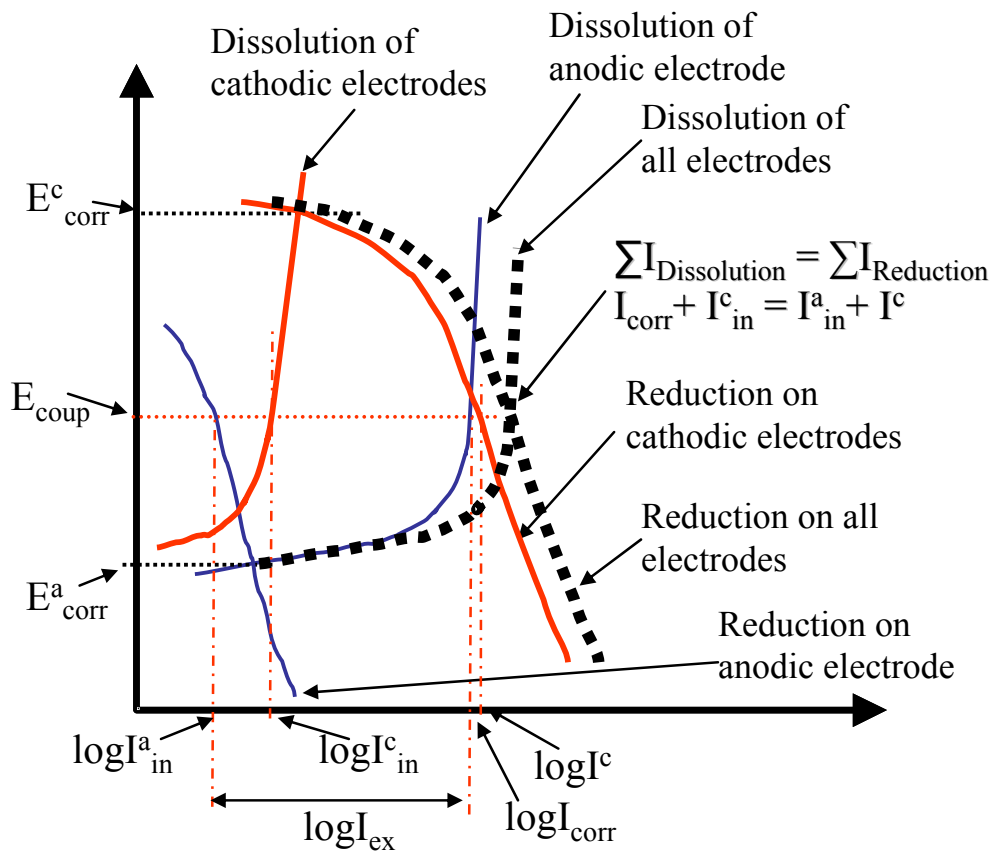
Figure 2. Schematic diagram for the polarization curves on the most anodic electrode and several cathodic electrodes that are connected together on a coupled multielectrode array sensor.
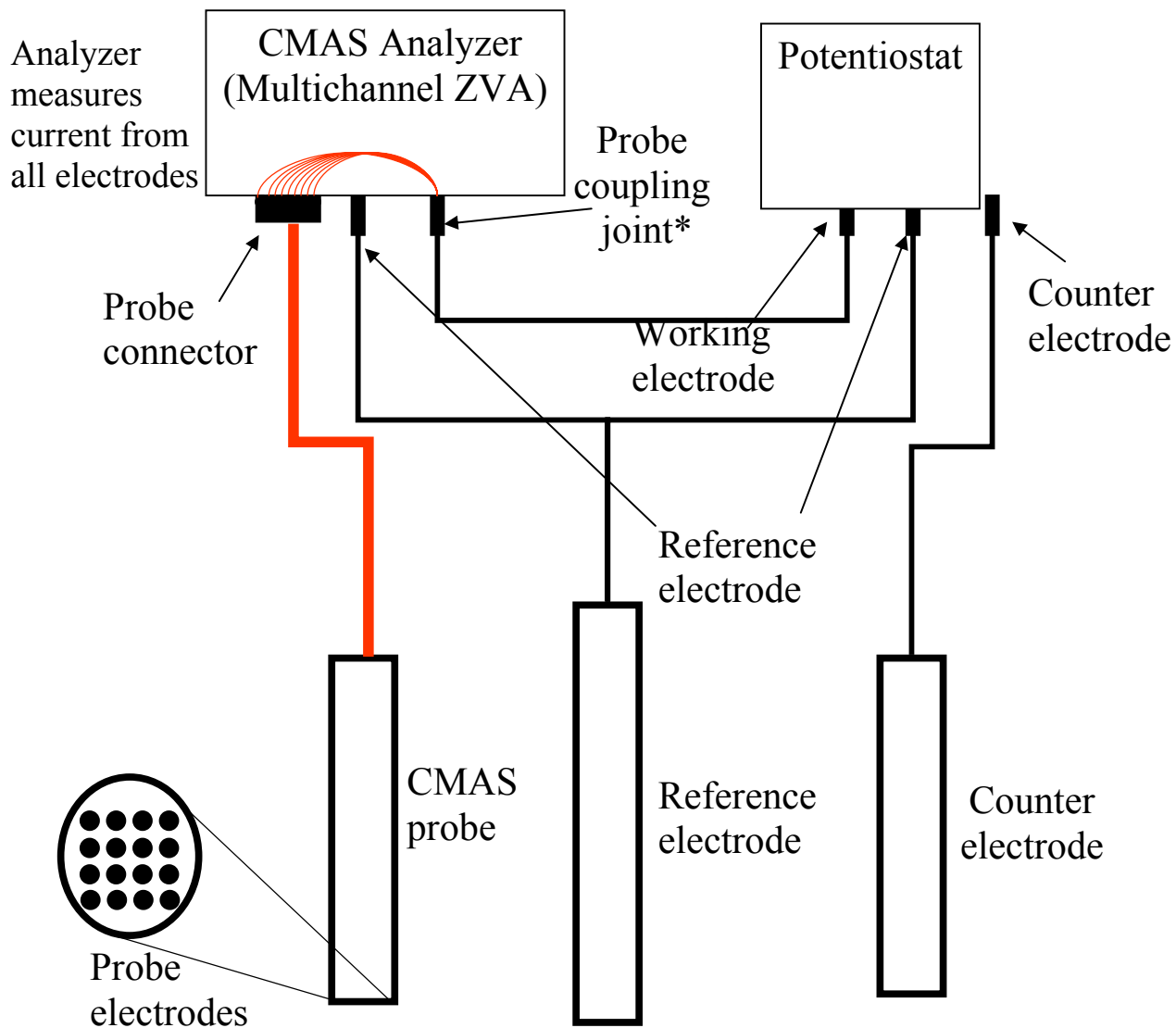
Figure 3. Experimental setup for studying the electrochemical behavior and internal current of the most anodic electrode in a CMAS probe. Note: The CMAS analyzer acted as a multichannel zero-voltage ammeter (ZVA) during the polarization test., Note: Probe coupling joint of CMAS analyzer is at the same potential of the probe electrodes
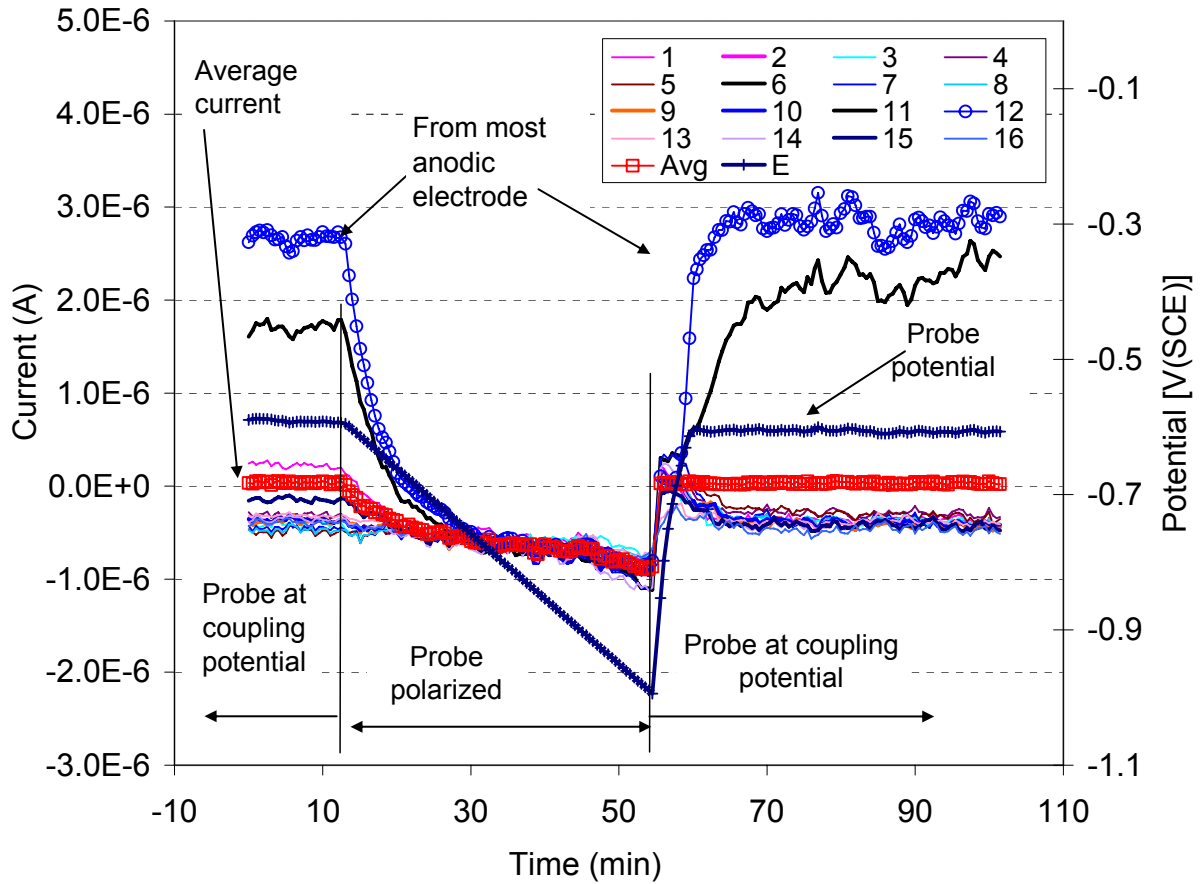
Figure 4. Probe potential and individual currents from a 16-electrode carbon steel probe in 3% NaCl solution prior to, during, and after the cathodic polarization in simulated seawater. Note: The average current was the average value of currents from the 16 electrodes. The numbers shown in the legend are the identification numbers for the electrodes of the probe, and E is for the probe potential. The currents from the electrodes that are not identified explicitly show the trend and variations only.
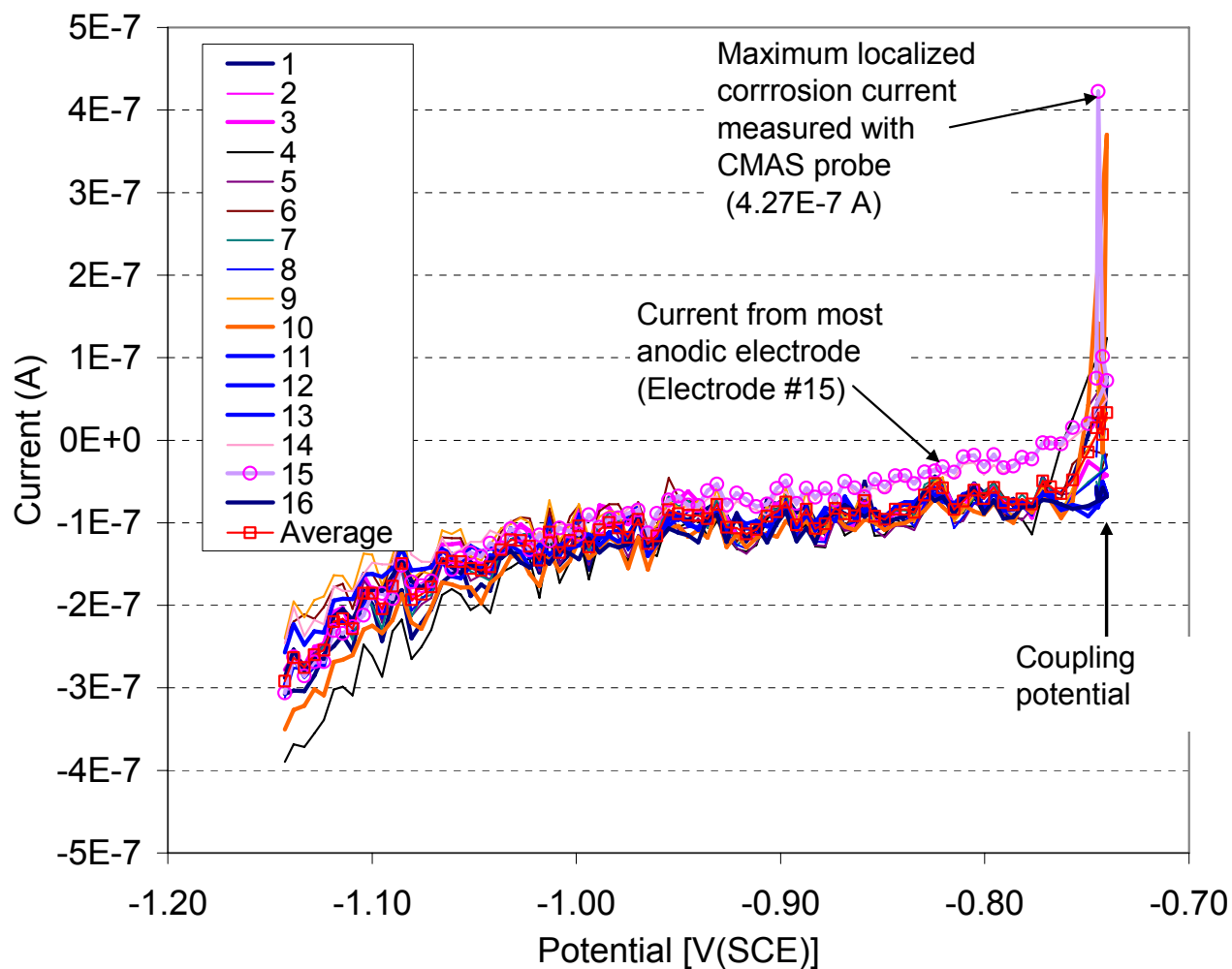
Figure 5. Typical current-potential curves for the electrodes on an aluminum CMAS probe in an air-saturated, simulated seawater solution. Note: Polarization was from the coupling potential toward the cathodic direction; the numbers shown in the legend are the identification numbers for the electrodes of the probe. The currents from the electrodes that are not identified explicitly show the trend and variations only.
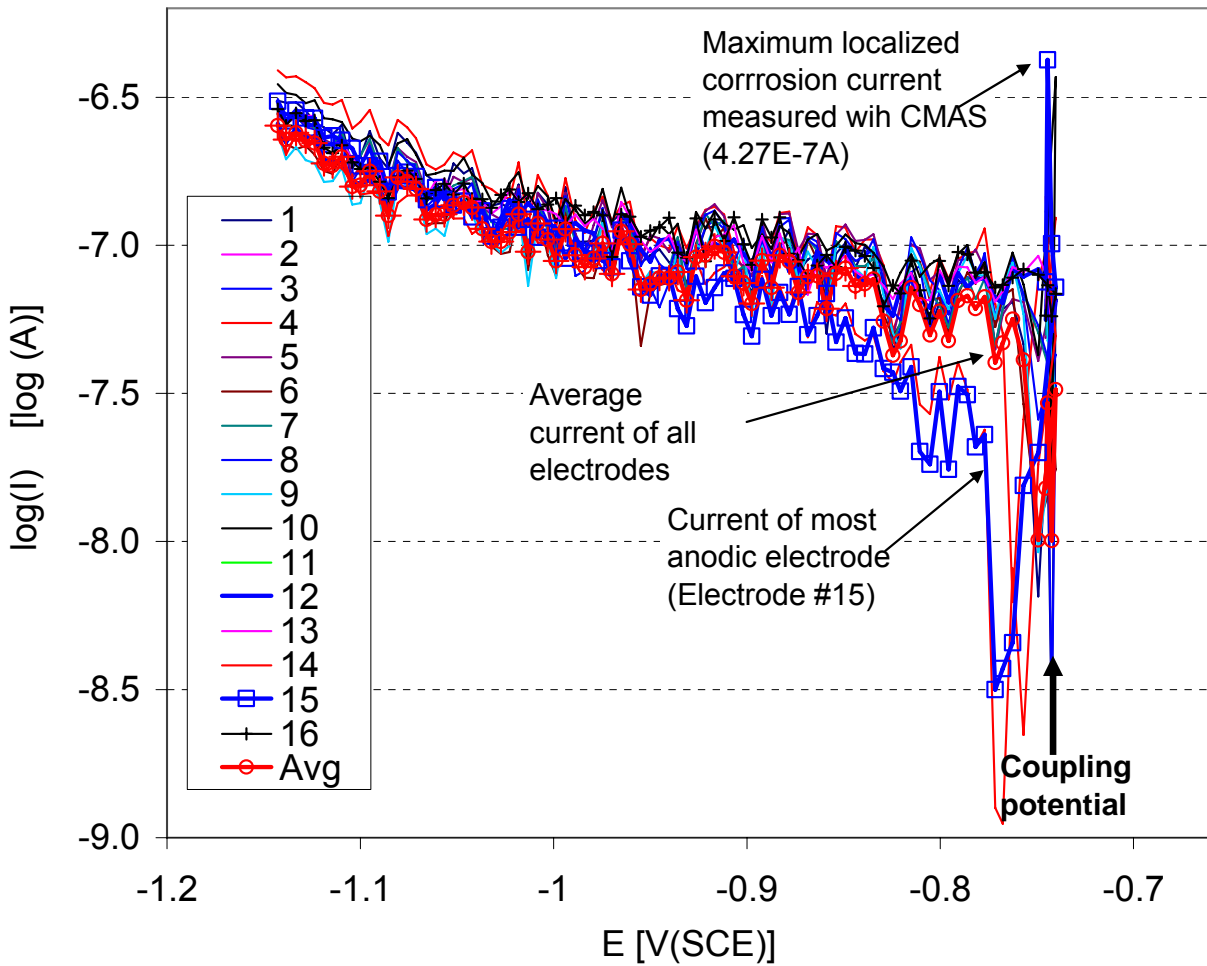
Figure 6. Typical logarithm polarization curves for the electrodes on an aluminum CMAS in an air-saturated and simulated seawater solution. Note: Polarization was from the coupling potential toward the cathodic direction; the numbers shown in the legend are the identification numbers for the electrodes of the probe. The currents from the electrodes that are not identified explicitly show the trend and variations only.
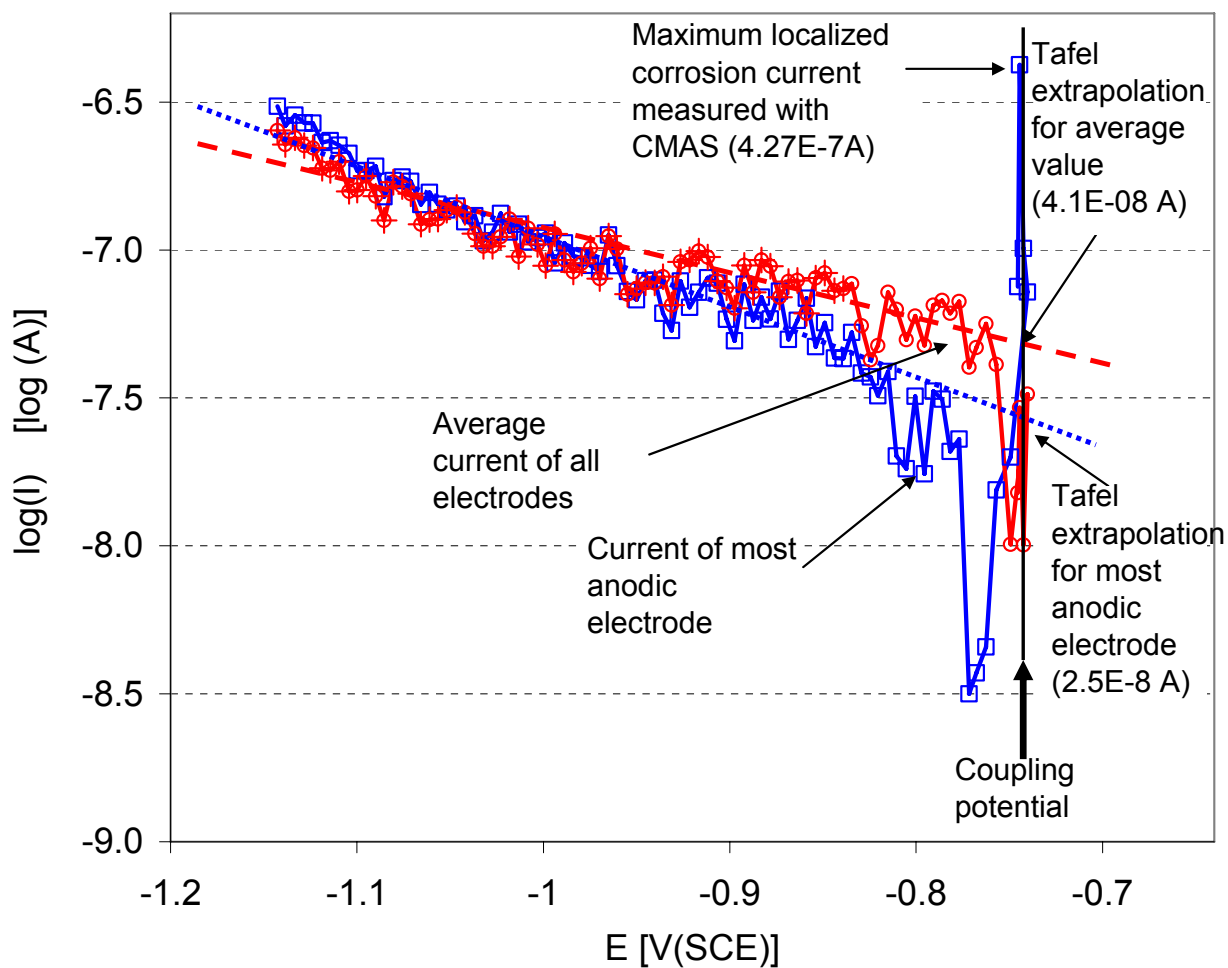
Figure 7. Polarization curves and Tafel extrapolation parameters for the current from the most anodic electrode and for the average current of all electrodes for the aluminum CMAS probe in simulated seawater.
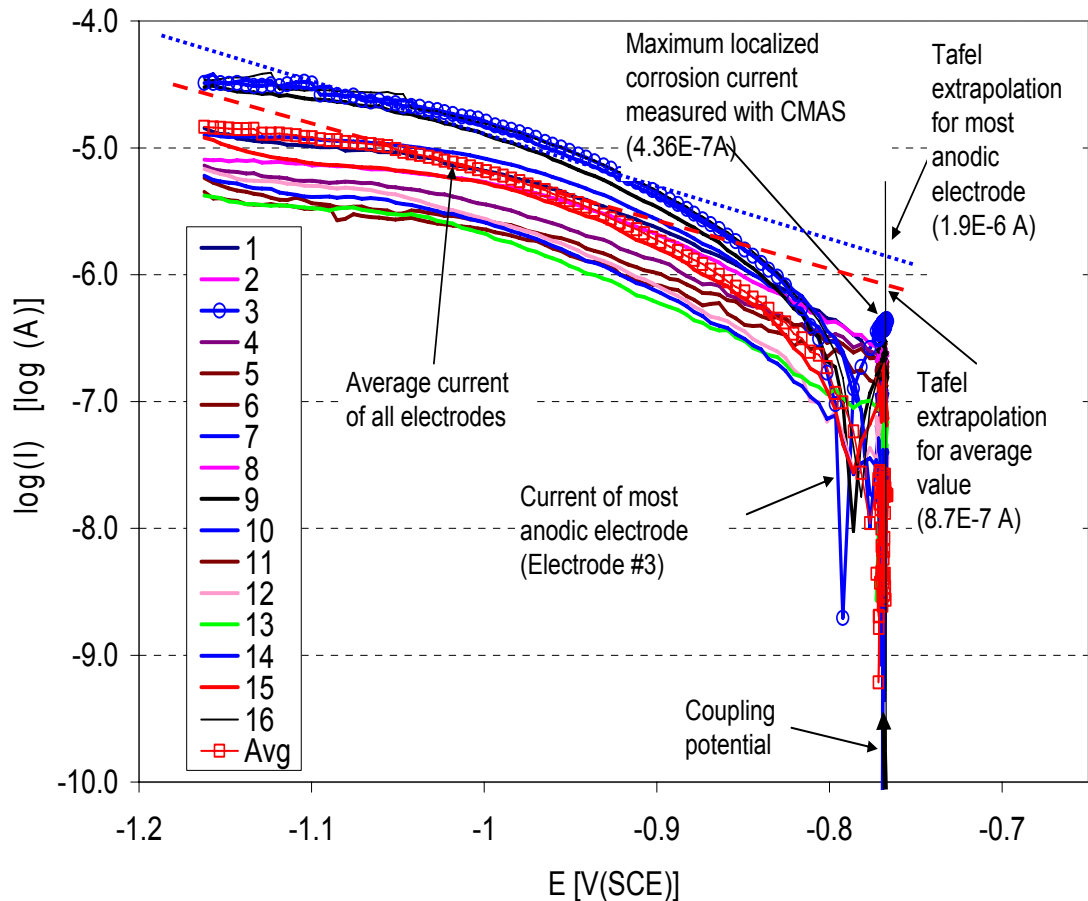
-4.0

-5.0

-6.0

log(I) [log (A)]

-7.0

-8.0

-9.0

-10.0

Maximum localized
corrosion current
measured with CMAS
(4.36E-7A)

Tafel
extrapolation
for most
anodic
electrode
(1.9E-6 A)

Average current
of all electrodes

Current of most
anodic electrode
(Electrode #3)

Tafel
extrapolation
for average
value
(8.7E-7 A)

Coupling
potential

Legend:
1
2
3
4
5
6
7
8
9
10
11
12
13
14
15
16
Avg

-1.2   -1.1   -1   -0.9   -0.8   -0.7

E [V(SCE)]

Figure 8. Typical polarization curves for the electrodes on the aluminum CMAS probe in an air-saturated 0.2 wt% hydrochloric acid solution and the Tafel extrapolation parameters for the current from the most anodic electrode and the average current. Note: Polarization was from the coupling potential toward the cathodic direction; the numbers shown in the legend are the identification numbers for the electrodes of the probe. The currents from the electrodes that are not identified explicitly show the trend and variations only.
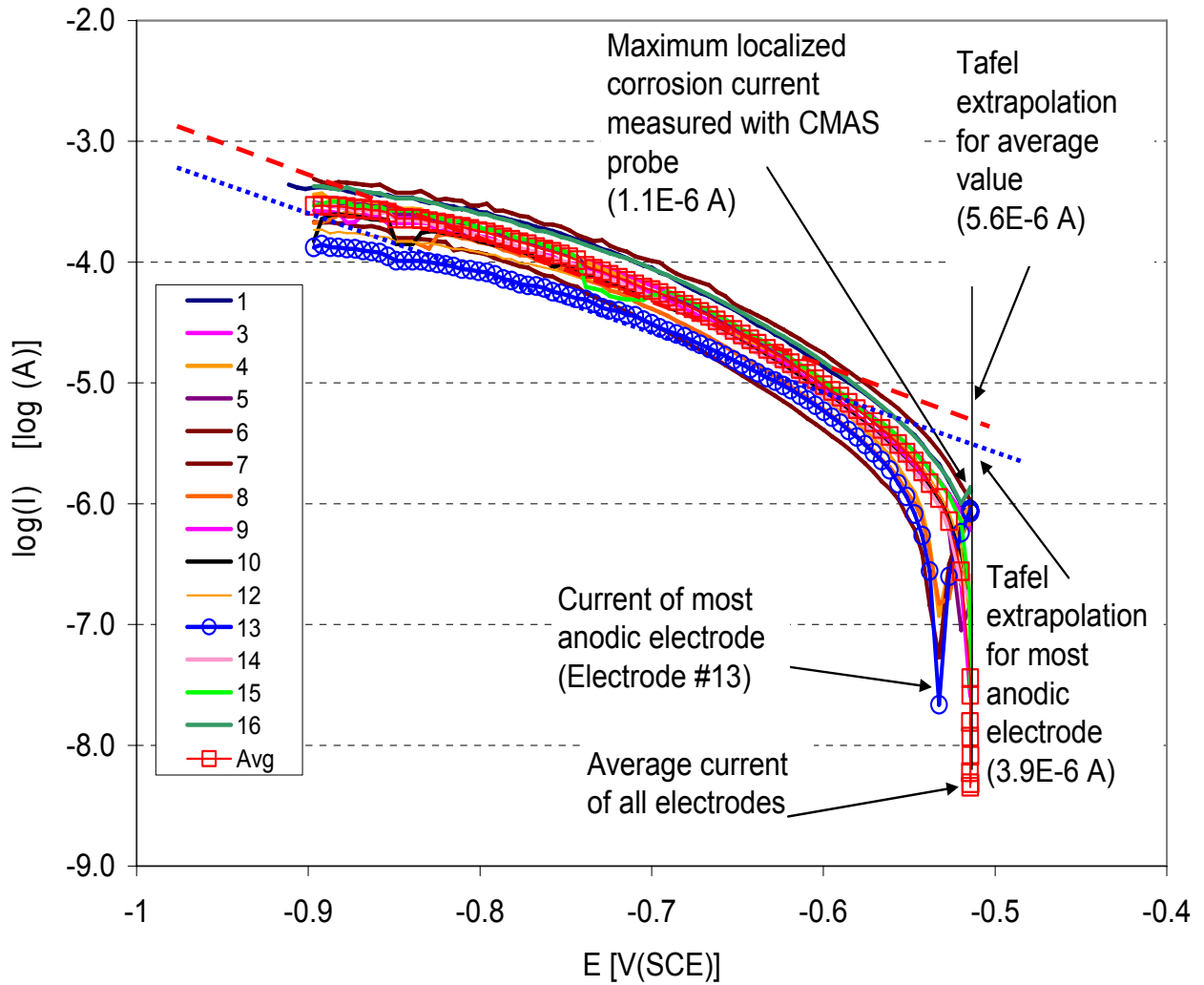
Figure 9. Typical polarization curves for the electrodes on the carbon steel CMAS probe in an air-saturated 2 wt% HCl solution and the Tafel extrapolation parameters for the current from the most anodic electrode and the average current. Note: Polarization was from the coupling potential toward the cathodic direction; the numbers shown in the legend are the identification numbers for the electrodes of the probe. The currents from the electrodes that are not identified explicitly show the trend and variations only.
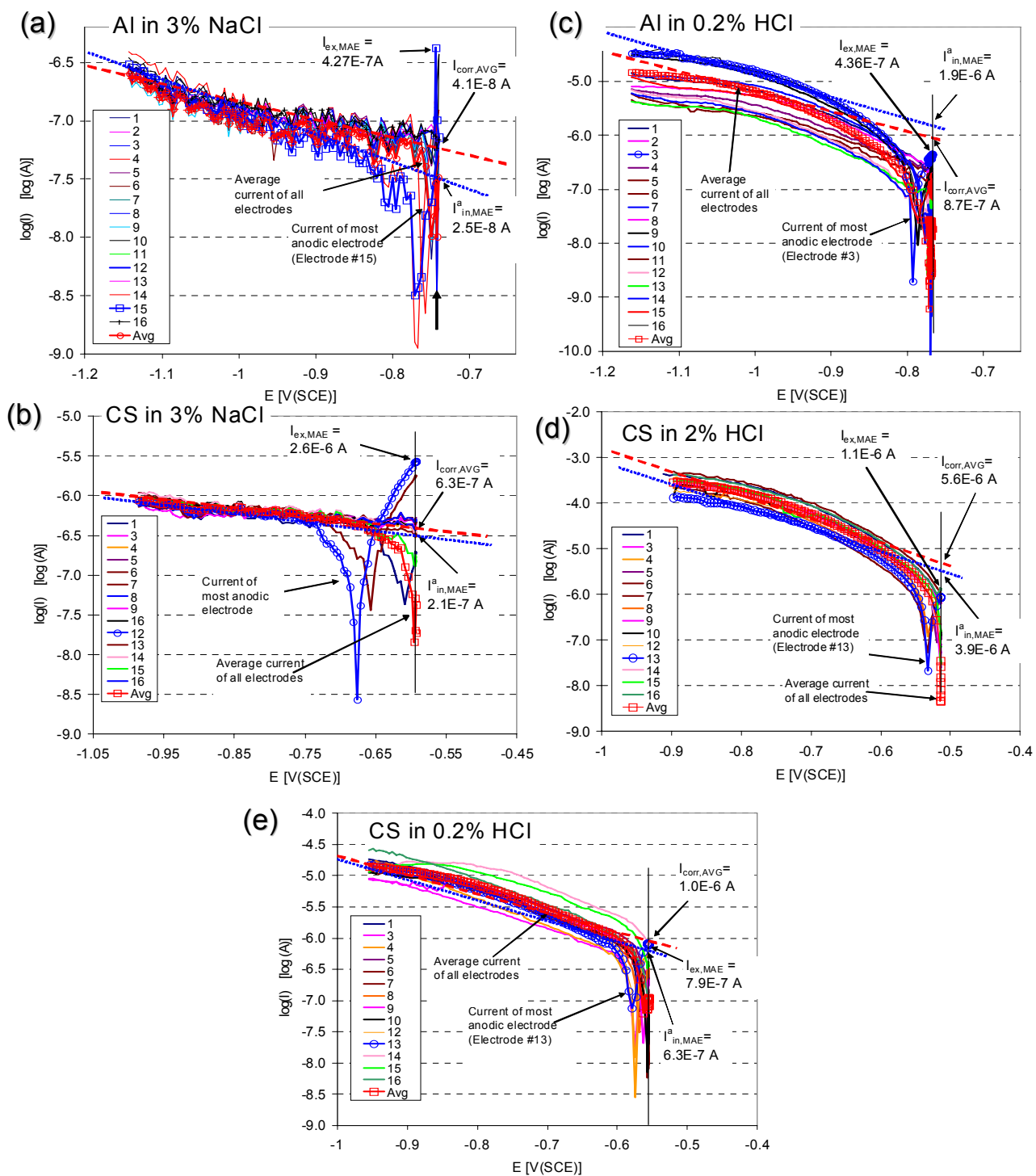
Figure 10. Comparison of the polarization behaviors for (a) aluminum in 3 wt% NaCl—localized corrosion dominant, (b) carbon steel in 3 wt% NaCl—non-uniform corrosion dominant, (c) aluminum in 0.2 wt% HCl—uniform corrosion dominant, (d) carbon steel in 2 wt% HCl—uniform corrosion dominant, and (e) carbon steel in 0.2 wt% HCl—uniform corrosion dominant.